Size-Selected Nanoparticle Chemistry: Kinetics of Soot Oxidation

Kelly J. Higgins,[†] Heejung Jung,[‡] David B. Kittelson,[‡] Jeffrey T. Roberts,*[,†] and Michael R. Zachariah*[,†,‡]

Department of Chemistry, University of Minnesota, 207 Pleasant Street SE, Minneapolis, Minnesota 55455, and Department of Mechanical Engineering, University of Minnesota, 111 Church Street SE, Minneapolis, Minnesota 55455

Received: December 11, 2000; In Final Form: October 3, 2001

A new experimental method has been developed to conduct surface chemistry and extract surface kinetic rates on size-selected nanoparticles. The method utilizes a tandem differential mobility analyzer (TDMA) technique in which monodisperse particles are selected from a polydisperse aerosol input stream and then subjected to chemical processing. The change in particle size is measured and used to determine kinetic information for the relevant surface reaction. The method has been applied to measure the oxidation rate of soot in air over the temperature range 800−1120 °C. Soot was generated in situ using an ethylene diffusion flame and sent to a differential mobility analyzer (DMA) to extract monodisperse particles. Three initial particle sizes of 40, 93, and 130 nm mobility diameter were subjected to oxidation in a high-temperature flow reactor, and the resulting change in particle size was measured with a second DMA. The measured size decreases were fit to a model utilizing a modified Arrhenius expression for the rate of decrease: $\dot{D}_p = -A_{nm}T^{1/2}\exp(-E_a/(RT))$. The fit yielded an activation energy of $E_a = 164$ kJ mol^{-1} with a different preexponential factor, A_{nm}, for each initial particle size. The size-decrease rates, and therefore the preexponential factors, differed by a factor of 1.7 between the 40 and 130 nm particles, with the 130 nm particles decreasing faster than the 40 or 93 nm particles. This may be the result of several factors including different effective densities or different soot particle compositions. The current experiments are the first measurements of the soot oxidation rate to be performed on size-selected, freshly generated soot particles using online aerosol techniques. Our results agree well with previous work over the temperature range covered, which is somewhat surprising given the wide range of techniques and materials previously studied in the effort to understand soot oxidation.

Introduction

Many important industrial processes produce nanoparticles either as unwanted byproducts or as desired end products. Virtually every combustion system from laboratory burners to coal-fired power plants and diesel engines produces soot nanoparticles as unwanted pollution. Nanoparticles can form in the process equipment used to fabricate microelectronic devices and ruin the devices if deposited on their surface. Novel catalysts and materials can be prepared using nanoparticle technology. In all of these systems, surface reactions that dictate growth and disappearance of the particles play a key role in determining the physical characteristics of the nanoparticles that are formed. In addition, nanoparticles play an important role in the chemistry of the atmosphere.[1] While the majority of the volume and mass of atmospheric particles is contained in particles with diameters between 0.1 and 10 μm, the greatest number count occurs for particles ∼10 nm in diameter, and most of the surface area of atmospheric particles is carried by particles less than 500 nm in diameter.[2] Given this, and the possible important changes in particle behavior with decreasing size, it is important to develop methods to probe the surface reactions of nanometer-sized particles as a function of their size. Toward this end, we have chosen the high-temperature oxidation of soot as a model system by which to study surface reactions on size-selected nanoparticles.

Soot production in combustion systems is a research area of much past and current interest.[3] Once soot nucleation has occurred, the amount of soot generated is determined by the competing processes of growth through the addition of gas-phase species and destruction through oxidation by O_2, OH, and other gas-phase oxidants. To understand and model soot production, it is necessary to obtain a molecular-level understanding of these processes. This includes, as a start, measuring oxidation and growth rates as functions of temperature and chemical composition. It is the purpose of the current study to present a new method for obtaining information on fundamental surface processes on nanoparticles, starting with the high-temperature oxidation of soot in air.

There have been many studies relevant to soot oxidation in the past, beginning with early work on the oxidation of carbon filaments,[4] carbon or graphite rods,[5,6] coal char,[7] and soot in a flame.[8] More recent work has used various manufactured carbon blacks as soot models and employed a variety of techniques including shock tubes,[9] thermogravimetric analysis,[10,11] and immobilized beds.[12] Studies using real laboratory-generated flame or diesel soot have been confined to techniques that rely on collecting and immobilizing the soot,[12,13] or light scattering or absorption within a flame environment.[14]

Each of the previous approaches to measuring the rate of soot oxidation by O_2 has drawbacks. Carbon and graphite do not contain hydrogen, oxygen, or nitrogen, all present in small

* To whom correspondence should be addressed. E-mail for J.T.R.: roberts@chem.umn.edu. E-mail for M.R.Z.: mrz@me.umn.edu.
† Department of Chemistry.
‡ Department of Mechanical Engineering.

10.1021/jp004466f CCC: $22.00
Published on Web 12/06/2001

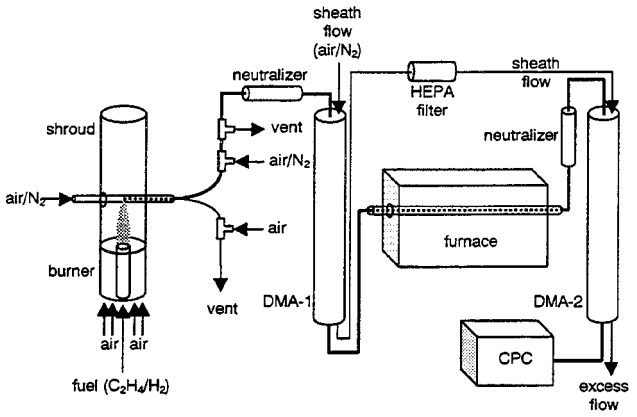

Figure 1. Schematic diagram of the experimental apparatus. The bold line indicates the path taken by the soot particles.

amounts in flame soot and all possibly important in determining the oxidation rate. Manufactured carbon blacks also may not be good models for freshly generated soot, as aging may change the surface characteristics of the particles. Immobilizing soot leads to difficulties in separating diffusion effects from reaction effects, while studying the oxidation in a flame environment cannot differentiate between oxidation by O_2 and oxidation by other species present in the flame such as OH. In addition, all of the previous studies worked with polydisperse soot size distributions and therefore were unable to explore possible size-dependent effects.

We report a new approach to the study of the oxidation of soot by O_2 using soot freshly generated in an ethylene diffusion flame and a tandem differential mobility analyzer (TDMA) to measure the decrease in size of monodisperse soot particles exposed to an oxidative environment. The TDMA technique has been used extensively in the past to measure minute particle-size changes associated with the hygroscopic and deliquescent properties[15] and the condensation or evaporation of aerosols,[16] while being used less often to measure particle-size changes due to reactive processes. McMurry et al. studied the reaction between ammonia gas and sulfuric acid aerosols by measuring the hygroscopic and deliquescent properties of the product aerosols.[17] Recently, Franz et al. used a TDMA apparatus in conjunction with a thermolysis tube to study the effect on diesel soot particles of H_2O_2 addition to the exhaust stream.[18] Their measurements were concerned with the evaporation of the volatile fraction of the particles and were only performed up to a thermolysis temperature of 650 °C.

Experimental Section

A diagram of the apparatus used in the present experiments is presented in Figure 1. In brief, polydisperse soot particles were generated in a diffusion flame and then sent to a differential mobility analyzer (DMA) for size selection. The produced monodisperse soot particles were then subjected to oxidation by air in a high-temperature furnace, and the resulting size changes were monitored using a second DMA with a condensation particle counter (CPC) as a particle detector. The details of each subsystem are as follows:

Soot Source. The soot was generated in a Santoro-type diffusion burner.[19] It consists of two concentric tubes: a 4 in. outer brass cylinder for air flow and a 0.5 in. inner brass tube for fuel flow. Between the concentric tubes is a honeycomb and a stack of beads and mesh to provide a uniform exit flow profile for the air. A 10 in. high glass cylindrical shroud is placed on the outer tube to prevent the flame from being disturbed by

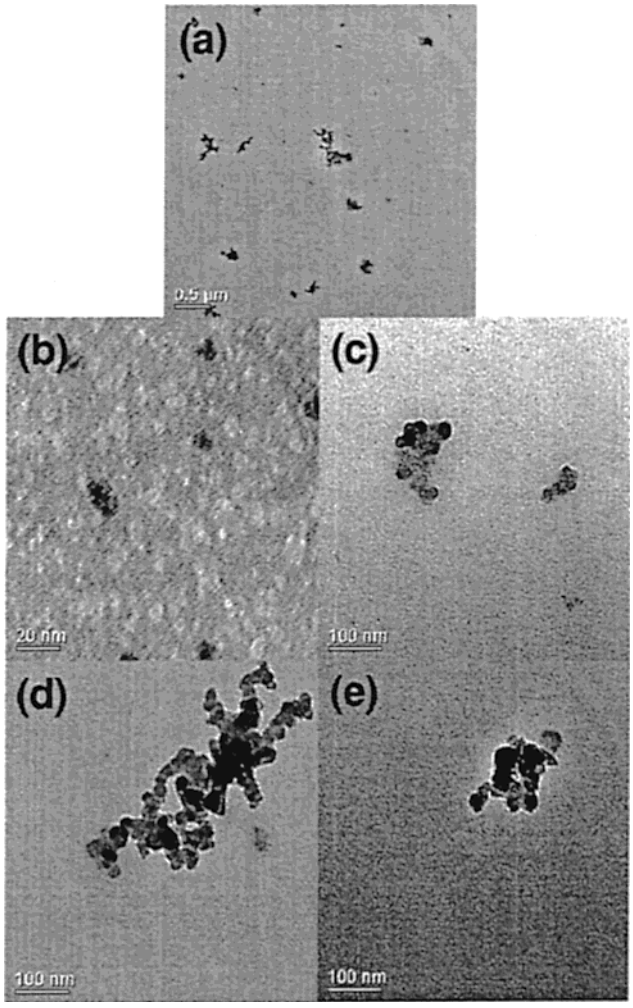

Figure 2. TEM images of soot particles generated in the ethylene diffusion flame and collected by quickly passing a carbon-film TEM grid through the tip of the flame (a−d) or by holding the grid for ∼10 s in one of the vent streams (e). Panel a gives an overview of the sizes and shapes of typical soot particles, panel b shows the primary particles sizes, and panels c and e show particles in the size range of this study, while panel d shows a much larger soot agglomerate.

outside air currents. For the current experiments, ethylene (Matheson, polymer grade) was used at a flow rate of 85 cm^3 min^{-1} to produce a flame 50 mm high.

The probe system used in this study is similar to one described by Kasper et al.[20] It consists of a horizontally fixed stainless steel tube with an inner diameter of 11 mm and a 1 mm orifice drilled in its bottom. Soot particles are collected through the 1 mm orifice and diluted and cooled by a 20 L min^{-1} flow of carrier gas. The sampling flow rate is determined by the pressure difference between the flame and the carrier gas stream, which flows at a slightly reduced pressure. For all of the air flows in the current oxidation experiments, air was supplied by the house compressed air system and was cleaned, dried, and filtered before use. Transmission electron microscopy (TEM) images of soot particles collected directly in the flame or in the sampling stream are shown in Figure 2. It can be seen that the soot particles are agglomerates of spherical particles with primary particle diameters of 20−30 nm.

Soot Size Selection. Because soot particles generated in the flame are highly charged with many more multiply charged particles than an equilibrium charge distribution, the entrained soot particles were passed through a ^{210}Po bipolar diffusion charger (neutralizer) to establish a known equilibrium charge

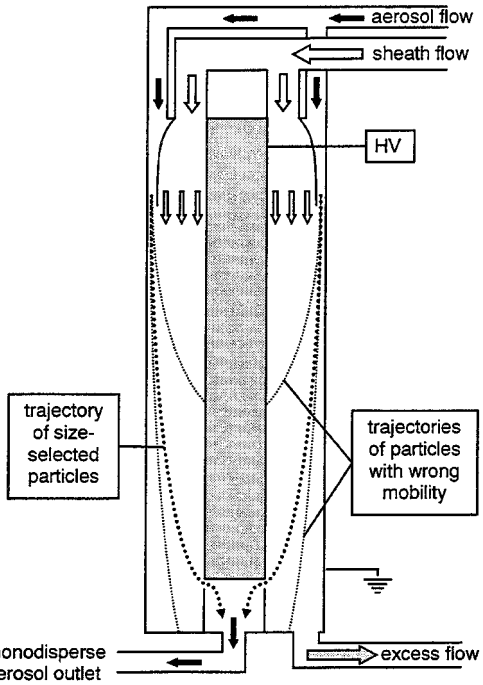

Figure 3. Schematic view of the DMAs used in this work. Particles with mobilities outside the desired range either hit and stick to the center rod electrode or go past the sampling slot and are carried away in the excess flow.

distribution. Differential mobility analyzers select size based on electric mobility, which is related to the drag and charge on a particle, rather than on absolute particle size. This means larger particles with multiple charges will pass through at the same voltage setting as the singly charged particles of the size of interest, much like a mass spectrometer will pass ions of the same mass-to-charge ratio. Although selecting multiple discreet sizes has the advantage of allowing one to track size-dependent effects in one experiment, in the present case the extent of size reduction and broadening of the peaks caused by oxidation served to blend the individual peaks together to such an extent that data analysis became extremely difficult. Thus, for all of the current experiments a neutralizer was used between the flame and DMA-1.

After the neutralizer, the soot particles were passed to DMA-1 (L = 44.413 cm, R1 = 0.945 cm, R2 = 1.924 cm). The details of DMA operation as both a monodisperse particle source[21] and as a particle size distribution measuring[22] tool have been presented previously. A DMA, illustrated schematically in Figure 3, consists of a center rod upon which a voltage is placed and an outer cylinder held at ground. The sheath flow is introduced at one end and flows coaxially between the outer cylinder and the inner rod. Aerosol particles enter the DMA in a thin ring adjacent to the outer cylinder, and the charged particles are attracted or repelled by the potential on the center rod. Near the end of the center rod is a slit through which particles of the desired electric mobility pass, while particles of higher electric mobility (particles that are smaller and/or more highly charged) hit the center rod upstream of the sample slit and particles of lower electric mobility (larger and/or uncharged) pass out of the DMA through the excess output flow. If the DMA is used to select a particular particle size, the center rod is held fixed at a voltage and the sample output flow will contain only particles of a single electric mobility. For the particle sizes used in the current experiments, the vast majority of charged particles in an equilibrium charge distribution will carry a single charge,[23] so the output aerosol will be essentially monodisperse.

TABLE 1: Flow Rates

flow description	value
Burner/Soot Sampling System	
fuel (C_2H_4)	85 cm^3 min^{-1}
carrier gas (air or N_2)	20 L min^{-1}
flame air	50 L min^{-1}
DMA-1	
polydisperse aerosol inlet	1.0 L min^{-1}
monodisperse aerosol outlet	1.0 L min^{-1}
sheath inlet (air or N_2)	10.0 L min^{-1}
excess outlet	10.0 L min^{-1}
DMA-2	
processed aerosol inlet	1.0 L min^{-1}
monodisperse aerosol outlet	1.0 L min^{-1}
sheath inlet (from DMA-1 excess)	10.0 L min^{-1}
excess outlet	10.0 L min^{-1}

If the DMA is used to measure the size distribution of a particle stream, the voltage on the center rod is stepped and the sample output flow is monitored for particle concentration as a function of applied voltage.

In the current TDMA experiments, DMA-1 was used to produce a monodisperse particle output stream from the polydisperse input stream. As seen in Figure 2, soot particles are geometrically complicated agglomerates of smaller particles, therefore the meaning of size used here is not straightforward. In the free-molecular and transition regimes, where the particle size is smaller than or comparable to the mean free path of the gas molecules (~65 nm for air at room temperature and one atmosphere), it has been shown that the particle mobility is inversely proportional to the mass transfer rate to the particle, which in turn is proportional to the gas-accessible surface area of the particle.[24] Therefore, for the particle sizes under consideration in this work, the DMA will select particles on the basis of their accessible surface area rather than a projected surface area as would be the case with much larger particles. The particle size is still described by a mobility diameter, D_p, which is the diameter of a spherical particle of equivalent mobility and therefore of the same surface area.

DMA-1 was operated at one of three voltages to size select D_p = 40, 93, and 130 nm particles, respectively. Flow rates used for DMA-1 and DMA-2 are listed in Table 1. It was found that to provide a constant sheath flow rate three stages of pressure regulation were required to damp out variations in the house air pressure. With one stage of pressure regulation, the center of the selected size distribution varied by about 5% over the cycle, while with three stages of pressure regulation the center varied negligibly. The excess flow output was sent through a HEPA filter to remove the nonselected soot particles and then used as sheath air input for DMA-2.

Flow Tube and Furnace. Monodisperse soot particles were sent to a tube reactor and furnace for oxidation. The quartz flow tube of 1.0 cm i.d. (1.2 cm o.d.) × 120 cm was prepared by washing with acetone, followed by baking at 1100 °C in the furnace until particle production ceased (~1 h). The quartz tube is suspended at the center of a 2.5 cm i.d. aluminum oxide tube, which is placed in a tube furnace (Lindberg model 55122 with 58114 temperature control). This arrangement reduces hot spots in the flow tube that may be caused by uneven furnace heating elements or by contact between the aluminum oxide and quartz tubes. The furnace is 50 cm long with a heated length of 30 cm. A bypass line around the furnace was used to measure unoxidized particle concentrations at various times during the experiments.

The temperature profile in the quartz tube was measured using a K-type thermocouple (Omega). Measurements were made with

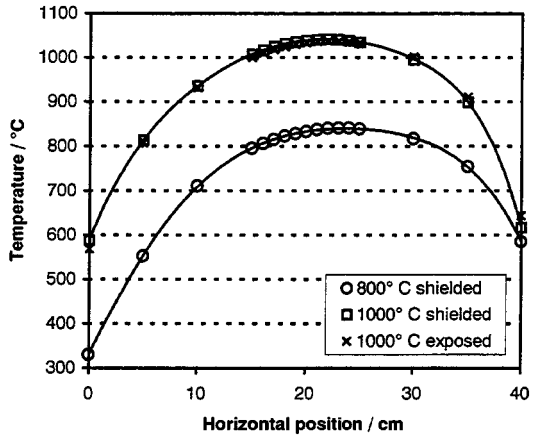

Figure 4. Temperature profiles within the quartz flow tube for furnace settings of 800 or 1000 °C. The data represented by open circles and squares were measured using a thermocouple shielded with a coil of iron wire, while the crosses show measurements made with an exposed thermocouple. The heated section of the furnace runs from a horizontal position of 5−35 cm.

the thermocouple junction exposed and with it shielded with a coil of iron wire to assess the effects of radiative heat transfer on the particle temperature. With the radiation shield in place the thermocouple measures the gas temperature, while with the 1 mm junction exposed to the tube walls, radiative heat transfer dominates and the thermocouple measures the wall temperature. Results of measurements made with the furnace set at 800 and 1000 °C and an air flow rate of 1.0 L min^{-1} through the tube are shown in Figure 4. There is very little difference between the shielded and exposed thermocouple results, indicating that the gas and wall temperatures are essentially the same. The peak temperature in the flow tube was typically 40 °C higher than the furnace setting.

Size Distribution Measurement. The resulting size distribution of the oxidized soot particles was measured using DMA-2 (same design as DMA-1) running in size-stepping mode with a condensation particle counter (CPC, TSI model 3760) detector. CPCs count nanoparticles by first passing them through a heated, saturated vapor of *n*-butanol and then allowing the *n*-butanol to condense onto the particles in a cooled region so that the particles grow to a size that scatters light efficiently. The particles then pass through a single-particle-counting optical detector, where they are detected by the pulse of scattered light as they cross a laser beam.

The aerosol input was taken directly from the flow tube output with no venting or dilution and run through a ^{210}Po neutralizer. As with the first neutralizer, preliminary experiments were run without a neutralizer between the flow tube and DMA-2. This is standard in TDMA experiments[15−17] because the majority of particles that pass through DMA-1 will have one positive charge, so it can be expected that a second neutralizer is not needed and in fact would diminish the signal at the CPC by as much as 90%. This is what we observed at lower furnace temperatures, but at temperatures above 500 °C, the signal begins to diminish significantly because of the apparent disappearance of the positive charge on the particles, so by 800 °C, the signal is 10% of that at 500 °C, and at 900 °C, there are no detectable particles. This same phenomenon was apparently observed in a previously published study of the effect of H_2O_2 on diesel soot[18] but was left without comment. The 3760 CPC requires on input flow rate of 1.415 L min^{-1}, so a small amount of make-up air is sampled through a filter from the room air to supplement the 1.0 L min^{-1} aerosol output of DMA-2.

The high-voltage supply for DMA-2 is remotely programmed using a PC with a multifunction board (National Instruments Lab-PC+) with a 12 bit D/A converter under software control. The output of the CPC is processed by a TSI 3703 remote processor, and the output of the 3703 is read through the serial port of the PC. Scans are performed by incrementing the particle size by 1 or 2 nm, waiting 10 s to allow the flow to stabilize, and then collecting 5 readings from the CPC at 2 s intervals. The 5 readings are averaged together to give the final data. The programmed voltage is calculated from the desired particle size using a standard equation.[16,22] The 12 bit resolution of the D/A converter can cause a significant mismatch between the programmed voltage and the actual voltage, leading to errors as large as 0.5 nm at the smaller particle sizes. To correct for this, the actual voltage supplied to DMA-2 has been measured at each of the particle sizes used in the experiments, and this voltage has been used to calculate the particle size measured for each particle size requested.

Experimental Procedure. The experimental procedure used was as follows: The flame was ignited, and all flows were set as previously specified. The system was allowed to stabilize for 1 h, at which point the flows were rechecked and the particle count for each size particle was measured using the bypass line. The flow was then rerouted through the flow tube, and scans of DMA-2 were made for each of the voltages of DMA-1. The furnace was set to the next temperature, and the system was allowed to equilibrate. This generally took about 15 min after the furnace temperature display reached the proper temperature and was monitored by tracking the decay in particle count at the peak of one of the previous size distributions. While the furnace was reaching the proper temperature, particle concentrations were measured for the three sizes with the flow going through the bypass line. Furnace settings ranged from 25 to 1100 °C, and all oxidation experiments reported here were performed in one 20 h session to reduce fluctuations due to atmospheric and other variations. During the course of the session, unoxidized particle concentrations measured through the bypass line around the furnace decreased by 60−70%.

To check for size reduction due to thermal effects such as particle collapse, rearrangement, or evaporation, experiments were run with the furnace set at 1100 °C using nitrogen (Airgas, industrial grade) as the soot-sampling carrier gas, the dilution gas, and the sheath gas for the two DMAs. All other conditions were kept the same as for the oxidation experiments.

Results and Analysis

Several corrections must be made to the raw CPC particle concentrations to determine the particle size distribution entering DMA-2. Particle-size-independent effects, such as the overall decrease in particle count, do not affect the peak position in the size distribution and were not corrected for here, whereas particle-size-dependent effects, such as charging and CPC counting efficiency, can change the peak position and appropriate corrections were applied as follows. The fraction of particles carrying a single positive charge in the equilibrium charge distribution created by the ^{210}Po neutralizer is a strong function of particle size. When the model developed by Fuchs is used,[23] approximately 4% of 10 nm particles and 22% of 100 nm particles will have one positive charge, while 91% of 10 nm particles and 43% of 100 nm particles will have no charge at all. To correct for this effect, we have used Wiedensohler's approximation[25] to Fuchs' model with the assumption that all of the particles in the peaks of interest were singly charged.

Another particle-size-dependent correction accounts for the combined detection efficiency of the CPC and transmission

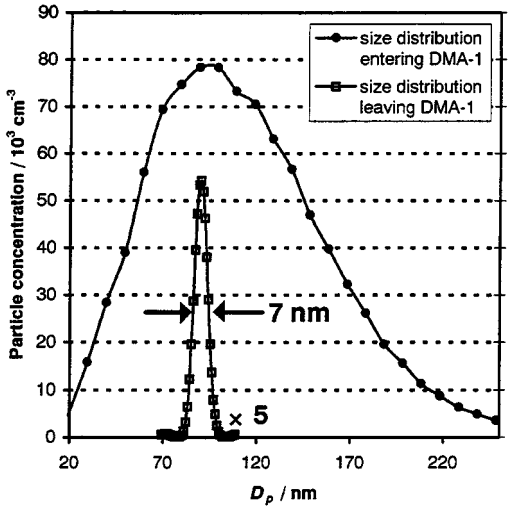

Figure 5. Single DMA scan of the overall soot particle size distribution sampled from the flame. Also shown is the particle size distribution after DMA-1 for the 93 nm size cut. Full width at half-maximum for this size cut is 7 nm. The large decrease in concentration is mainly due to the low percentage of positive, singly charged particles present at charge equilibrium for this size particle.

efficiency of the DMA. Wang and Flagan[26] measured the detection efficiency of the TSI 3760 CPC and the transmission efficiency of a TSI DMA similar in dimension to the DMAs used in this work, and we have used an approximation to their data to correct for the overall CPC/DMA efficiency. As can be seen in Figure 2 of ref 26, the combined efficiency is quite poor for particles below 13 nm, so the data have been truncated at a minimum particle size of 13 nm.

For the TDMA scans, peaks in the corrected particle size distribution were fit to a normal Gaussian function with the center of the Gaussian taken as the particle size and the area under the Gaussian taken as the total particle count. In most cases, a single Gaussian was used for each peak, but in cases in which peaks began to overlap or in which a bimodal distribution developed, multiple Gaussians were used.

Single DMA Results. The overall particle size distribution sampled from the flame was obtained by bypassing DMA-1, running the particles through the flow tube, and measuring the distribution using DMA-2 and the CPC. Results for a furnace setting of 25 °C are presented in Figure 5, along with a typical size cut at 93 nm. Setting the furnace at 1100 °C resulted in no particles being detected at the CPC, indicating that soot was completely oxidized away at that temperature.

Preliminary Tandem DMA Results. Initial broad TDMA scans, ranging from 15 nm to approximately twice the selected particle size, are presented in Figure 6. The scans for the 93 and 130 nm particles were performed at 25 °C, while the scans for the 40 nm particles were performed over a temperature range of 25−975 °C. The 40 nm particle data again show no evidence of particle break-up. These data also give an indication of the number of multiply charged particles passing through DMA-1 by comparing the two largest peaks. The peak at the higher size is from particles that were doubly charged in DMA-1 but were singly charged when passing through DMA-2. The largest peak is from particles of the size of interest that were singly charged in both DMA-1 and DMA-2, with a small contribution from larger particles that were doubly charged in both DMA-1 and DMA-2. The number of these larger particles in the main peak can be calculated from the size of the second peak by looking at the ratio of singly to doubly charged particles of the larger size in an equilibrium charge distribution. In each case, less than 10% of the main peak is due to the larger particles.

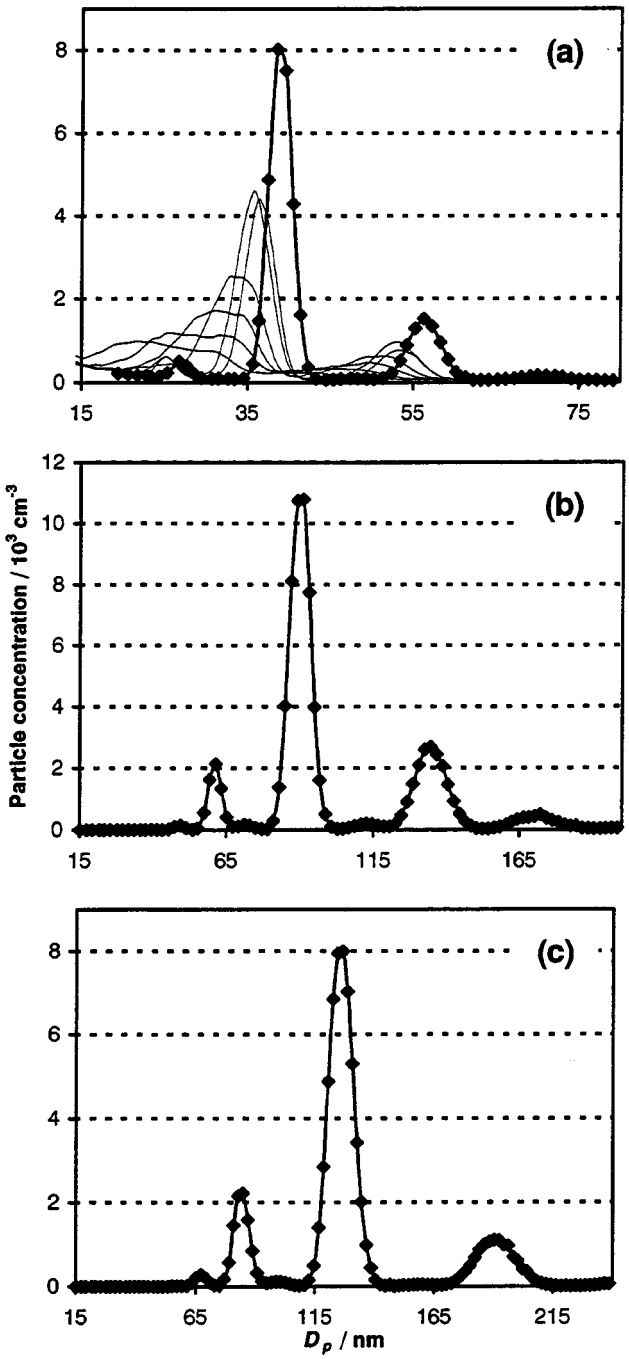

Figure 6. Broad TDMA scans at the three voltage settings of DMA-1 used in the experiments: (a) −281 V; (b) −1283 V; (c) −2282 V. Panel a shows scans at 25 °C (thick line) and, moving down and to the left of the 25 °C peaks, at 800, 850, 900, 925, 950, and 975 °C. Panels b and c show scans at 25 °C. The three largest peaks of each scan are identified from left to right as being due to doubly charged particles of the primary selected size, singly charged particles of the primary selected size, and particles that were doubly charged when passing through DMA-1 but were singly charged when passing through DMA-2.

The results from the experiments using nitrogen instead of air as the carrier gas are shown in Figure 7. The size decrease for each of the selected particle sizes is ∼2 nm at 1100 °C. In contrast, at this temperature in air all of the soot has disappeared. This indicates that thermal effects do not substantially alter the mobility diameter of the particles. Some restructuring may be taking place, but it does not significantly change the measured

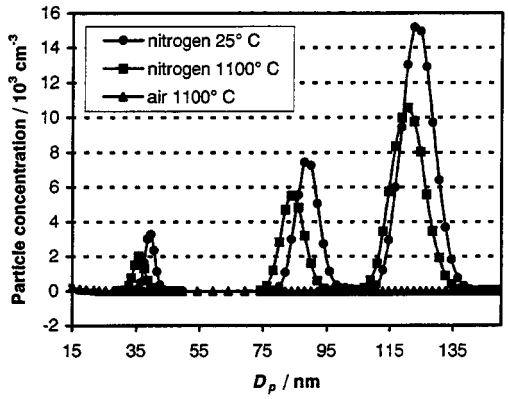

Figure 7. Results for the three particle sizes used in this study comparing the use of N_2 as the carrier gas with air as the carrier gas. Filled circles are at a furnace setting of 25 °C, while filled boxes are at a furnace setting of 1100 °C using N_2. Filled triangles are for air at 1100 °C.

particle size. This small size change may also be due to a thin layer of semivolatile material evaporating off of the surface of the particles.

Oxidation Results. The TDMA scans for the oxidation in air of the three initial soot particle sizes are presented in Figure 8. Measured size changes are presented in tabular form in Table 2. The initial ~1% decrease in D_p at 500 °C for all three particle sizes was most likely due to volatile or semivolatile material evaporating off of the particles, and the size decrease due to oxidation is calculated relative to the particle sizes at 500 °C. An increase in the width, or spreading, of the size distributions as oxidation occurs can be seen in Figure 8, along with the appearance of a bimodal distribution at higher temperatures for the 40 nm particles. What appears to be a bimodal distribution for the larger particles is actually a blending of the peak due to singly charged particles with the peak due to doubly charged particles.

Kinetic parameters can be obtained from the observed decreases in particle size using a modified form of the Arrhenius expression for the size decrease rate:

$$\dot{D}_p = -A_{nm} T^{1/2} \exp\left[-\frac{E_a}{RT}\right] \quad (1)$$

where A_{nm} is a size-dependent preexponential factor and E_a is a size-independent activation energy. Given experiments at a series of constant temperatures and a known residence time in the reaction region, one can straightforwardly calculate these parameters. The complication in the present study is a result of the nonuniform temperature profile in the reaction region of the flow tube, as seen previously in Figure 4.

To extract more accurate kinetic parameters, it is necessary to integrate the diameter change as a particle travels the length of the tube:

$$\Delta D_p = \int_0^X \frac{\dot{D}_p(x)}{u(x)}\,dx \quad (2)$$

where x is the horizontal position in the tube, X is the length of the tube, and u is the flow velocity. The dependence of the rate and flow velocity on horizontal position is a result of their dependence on temperature as seen in eq 1 and

$$u(x) = \frac{4}{3} u_m \frac{T(x)}{T_o} \quad (3)$$

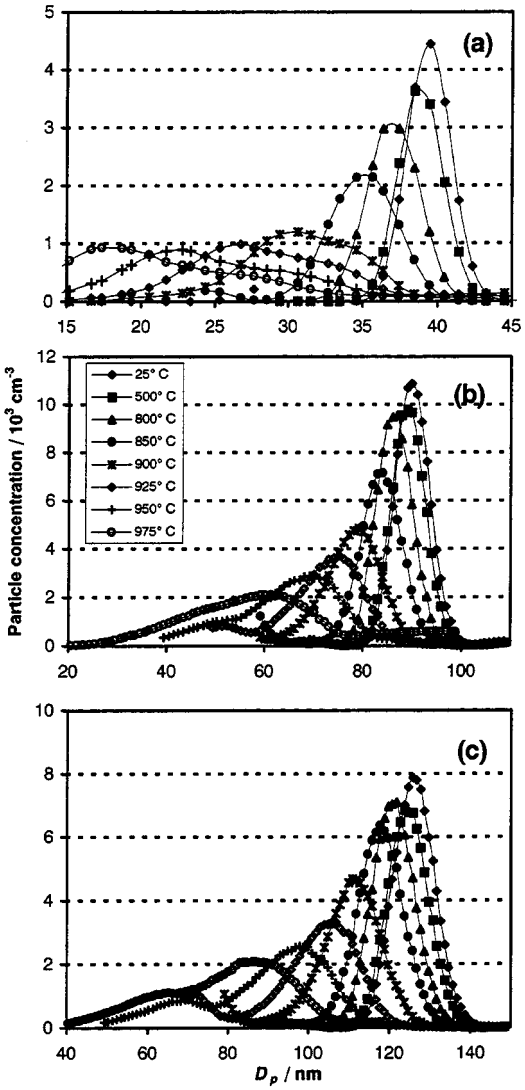

Figure 8. TDMA soot oxidation results in air for furnace settings of 25−975 °C (see legend). Results from higher furnace settings are omitted for clarity: (a) 40 nm initial particle size; (b) 93 nm initial particle size; (c) 130 nm initial particle size.

TABLE 2: Measured Particle Sizes

	initial and final particle size (nm)		
furnace setting (°C)	40	93	130
25	40.3	92.6	129.8
500	39.7	91.7	128.2
800	37.8	88.8	124.5
850	35.8	86.1	121.3
900	30.4	81.6	114.4
925	27.1	78.1	109.3
950	22.8	73.3	101.6
975	18.5	65.2	91.0
1000		48.8	75.3
1025		34.6	56.6
1050		19.6	35.9
1075			17.0

where u_m is the mean flow velocity calculated from the volume flow rate and the cross sectional area of the flow tube, and $^4/_3 u_m$ is the peak volumetric flow velocity assuming laminar flow.

A nonlinear least-squares fit to the experimental data was performed by numerically integrating eq 2 for each furnace setting and initial particle size combination. Temperature profiles for furnace settings other than 800 or 1000 °C were estimated using a linear interpolation or extrapolation of the points

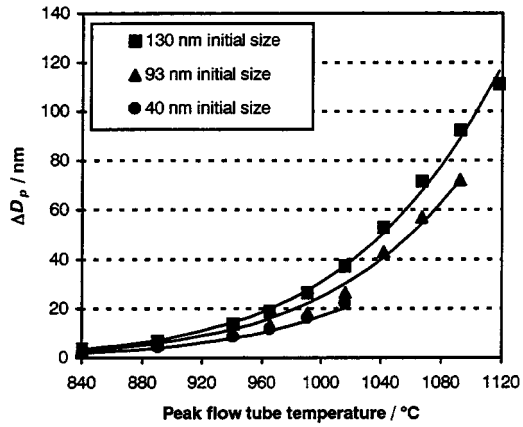

Figure 9. Particle size change as a function of peak flow tube temperature for the three initial particle sizes. Solid lines show size change calculated from the fitted model.

TABLE 3: Fitted Kinetic Parameters

parameter	value
E_a	164 kJ mol^{-1}
A_{40}	1.9×10^7 nm K$^{-1/2}$ s^{-1}
A_{93}	2.6×10^7 nm K$^{-1/2}$ s^{-1}
A_{130}	3.2×10^7 nm K$^{-1/2}$ s^{-1}

measured using the shielded thermocouple at 800 and 1000 °C, while interpolation for a specific furnace setting was performed by fitting the points measured at specific distances in the flow tube to a sixth-order polynomial. The values obtained for the parameters A_{40}, A_{93}, A_{130}, and E_a are listed in Table 3. Figure 9 presents the observed and calculated size decreases of the soot particles.

An attempt was made to fit the exponent of the temperature in eq 1, but this was highly correlated with the A_{nm} parameters and not determinable from our data. It was held fixed at 0.5 to roughly account for the dependence of collision frequency on temperature. Also, fitting with a single size-dependent A parameter was attempted, but no adequate functional dependence on particle size could be found to fit the data for all three initial particle sizes. This indicates that the differences in size decrease rate observed for the three initial particle sizes are most likely more a function of the initial particle structure than the absolute particle size.

The particle size decrease rate can be translated into an oxidation rate by first assuming the soot mass lost is equal to the mass lost by a sphere with the same density as soot undergoing the same diameter decrease. The mass lost is simply

$$\Delta m_s = \frac{\pi \rho_s}{6}(D_{p,i}{}^3 - D_{p,f}{}^3) \tag{4}$$

where $D_{p,i}$ and $D_{p,f}$ are the initial and final mobility diameters of the soot particle, m_s is the soot particle mass, and ρ_s is the mass density of the soot particle. The surface specific oxidation rate, $\dot{w}$, is defined as

$$\frac{dm_s}{dt} = -\dot{w}A_s \tag{5}$$

with A_s being the soot surface area. Using the approximation of spherical soot particles and integrating over the residence time τ, one gets

$$\dot{w} = \frac{\rho_s(D_{p,i} - D_{p,f})}{2\tau} = \frac{\rho_s}{2}\dot{D}_p \tag{6}$$

which relates the surface specific oxidation rate directly to the diameter decrease rate.

Discussion

The largest uncertainty in the present experiments comes from the assumption of laminar flow. Because of the horizontal orientation of the flow tube, buoyancy effects may cause the soot particles to take a complicated trajectory through the flow

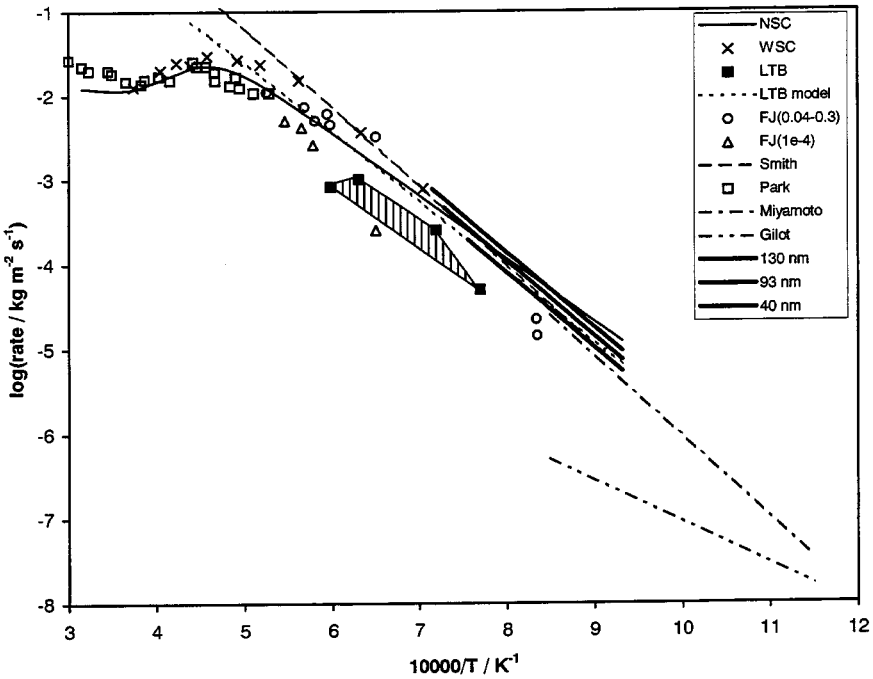

Figure 10. A comparison of the current work with selected prior work. The thick lines show the current work with the 40 nm particle results on the bottom and the 130 nm particle results on the top. A density of 1800 kg m^{-3} was used to calculate the surface specific rate from the particle diameter decrease rate. Prior work is from the following sources: NSC (ref 5), WSC (ref 6), LTB and LTB model (ref 8a), FJ (ref 8b), Smith (ref 7), Park (ref 9a), Miyamoto (ref 13a), and Gilot (ref 10).

tube, thereby increasing the residence time by as much as a factor of 2. This may not be a bad thing, because calculations assuming a laminar flow show a large spreading of the particle size distribution as the oxidation occurs due to the wide distribution in particle residence times in a laminar flow. If buoyancy effects cause significant randomizing of the particle trajectories, the differences in residence time will be reduced, thus giving a much smaller spreading of the particle size distribution. Experimentally, the observed spreading of the size distributions is more in line with the later residence time assumption. Either way, if we assume the uncertainty in the residence time is linear in residence time, it will translate linearly into an uncertainty in the A_{nm} parameters while leaving the activation energy the unchanged.

Comparison of the current results with selected past studies of soot oxidation shows good agreement, as can be seen in Figure 10. This is somewhat surprising given the wide range of techniques and materials employed in the previous and current studies. The level of agreement is further evidence that the observed size change of the soot particles is due to oxidation and not thermally induced particle rearrangement, collapse, or evaporation.

There is a factor of 1.7 difference between the measured oxidation rates of the 40 and 130 nm particles. This may be due to a difference in the effective densities of the soot particles[27] or in the composition of the particles. Because of the agglomerate structure of the soot particles, the effective density of the larger particles is lower than that of the smaller particles. This could lead to a higher rate of observed size reduction for the larger particles. Preliminary experiments in altering the soot composition indicate that increasing the amount of hydrogen in the soot leads to a higher oxidation rate. It can be conjectured that the different-sized particles have had different histories within the flame and thus might be expected to have different elemental composition.

Conclusion

We have demonstrated a new experimental method to conduct surface chemistry and extract surface kinetic rates on size-selected nanoparticles. This method, which utilizes a tandem differential mobility analyzer to measure the change in particle size due to surface chemical reactions, has been used to study the oxidation rate of soot nanoparticles in air over the temperature range of 800−1120 °C. Soot was generated in situ with an ethylene diffusion flame and characterized by online aerosol techniques before and after oxidation in a high-temperature laminar flow tube. Three initial particle sizes of mobility diameter 40, 93, and 130 nm were studied, and each was found to reduce in size due to oxidation at a different rate, with the 130 nm particles reducing in size 1.7 times faster than the 40 nm particles. An single activation energy of 164 kJ mol^{-1} was used to fit the temperature dependence of the observed rates for all initial particle sizes. The difference in apparent oxidation rate may be attributable to differences in effective densities, compositions, or both for the different initial particle sizes. The current study represents the first study of soot oxidation using freshly generated, size-selected soot particles and online aerosol processing techniques.

This same method is being applied to investigate the composition and oxidant-dependent oxidation rate of soot by varying the fuel used in the burner, and thus the composition of the soot particles, or by varying the oxidant in the carrier gas. With a better understanding of how composition and/or oxidant species affects the oxidation rate, a more detailed picture of the mechanism of soot oxidation can be gained. In addition, this method lends itself to studies of soot generated by real-world sources such as diesel engines. With the growing emphasis on reducing diesel particulate emissions, information on diesel soot burnout through oxidation will be quite valuable.

Acknowledgment. K.J.H. and J.T.R. would like to thank the Camille and Henry Dreyfus Foundation for support in the form of a Postdoctoral Fellowship in Environmental Chemistry.

References and Notes

(1) Finlayson-Pitts, B. J.; Pitts, J. N., Jr. *Atmospheric Chemistry: Fundamentals and Experimental Techniques*; John Wiley: New York, 1986; Chapter 12.

(2) Whitby, K. T.; Sverdrup, G. M. *Adv. Environ. Sci. Technol.* **1980**, *10*, 477.

(3) Kennedy, I. M. *Prog. Energy Combust. Sci.* **1997**, *23*, 95 and references therein.

(4) Strickland-Constable, R. F. *Trans. Faraday Soc.* **1944**, *40*, 333. Also reviews earlier carbon oxidation studies.

(5) Nagle, J.; Strickland-Constable, R. F. *Fifth Carbon Conference*; Pergamon: Oxford, 1962; Vol. 1, pp 154−164.

(6) Walls, J. R.; Strickland-Constable, R. F. *Carbon* **1964**, *1*, 333.

(7) Summarized in: Smith, I. W. *Nineteenth Symposium (International) on Combustion*; The Combustion Institute: Pittsburgh, PA, 1982; pp 1045−1065.

(8) (a) Lee, K. B.; Thring, M. W.; Beér, J. M. *Combust. Flame* **1962**, *6*, 137. (b) Fenimore, C. P.; Jones, G. W. *J. Phys. Chem.* **1967**, *71*, 593.

(9) (a) Park, C.; Appleton, J. P. *Combust. Flame* **1973**, *20*, 369. (b) Brandt, O.; Roth, P. *J. Aerosol Sci.* **1988**, *19*, 863. (c) Brandt, O.; Roth, P. *Combust. Flame* **1989**, *77*, 69. (d) Cadman, P.; Denning, R. J. *J. Chem. Soc., Faraday Trans.* **1996**, *92*, 4159.

(10) Gilot, P.; Bonnefoy, F.; Marcuccilli, F.; Prado, G. *Combust. Flame* **1993**, *95*, 87.

(11) Encinar, J. M.; González, J. F.; Sabio, E.; Rodríguez, J. J. *J. Chem. Technol. Biotechnol.* **2000**, *75*, 213.

(12) Neeft, J. P. A.; Nijhuis, T. X.; Smakman, E.; Makkee, M.; Moulijn, J. A. *Fuel* **1997**, *76*, 1129.

(13) (a) Miyamoto, N.; Zhixin, H.; Hideyuki, O. *SAE Technol. Pap. Ser.* **1988**, No. 881224. (b) Ahlström, A. F.; Odenbrand, C. U. I. *Carbon* **1989**, *3*, 475. (c) Du, Z.; Sarofim, A. F.; Longwell, J. P.; Mims, C. A. *Energy Fuels* **1991**, *5*, 214. (d) Ciambelli, P.; D′Amore, M.; Palma, V.; Vaccaro, S *Combust. Sci. Technol.* **1996**, *121*, 67.

(14) (a) Feugier, A. *Combust. Flame* **1972**, *19*, 249. (b) Neoh, K. G.; Howard, J. B.; Sarofim, A. F. In *Particulate Carbon: Formation During Combustion*; Siegla, D. C., Smith, G. W., Eds.; Plenum: New York, 1981; pp 261−282. (c) Garo, A.; Prado, G.; Lahaye, J. *Combust. Flame* **1990**, *79*, 226. (d) Schäfer, Th.; Mauss, F.; Bockhorn, H.; Fetting, F *Z. Naturforsch., A: Phys. Sci.* **1995**, *50*, 1009.

(15) Liu, B. Y. H.; Pui, D. Y. H.; Whitby, K. T.; Kittelson, D. B.; Kousaka, Y.; McKenzie, R. L. *Atmos. Environ.* **1978**, *12*, 99.

(16) Rader, D. J.; McMurry, P. H. *J. Aerosol Sci.* **1986**, *17*, 771.

(17) McMurry, P. H.; Takano, H.; Anderson, G. R. *Environ. Sci. Technol.* **1983**, *17*, 347.

(18) Franz, B.; Eckhardt, T.; Kauffeldt, T.; Roth, P. *J. Aerosol Sci.* **2000**, *31*, 415.

(19) Santoro, R. J.; Semerijan, H. G.; Dobbins, R. A. *Combust. Flame* **1983**, *51*, 203.

(20) (a) Kasper, M.; Siegmann, K.; Sattler, K. *J. Aerosol Sci.* **1997**, *28*, 1569. (b) Kasper, M.; Sattler, K.; Siegmann, K.; Matter, U.; Seigmann, H. C. *J. Aerosol Sci.* **1999**, *30*, 217.

(21) (a) Liu, B. Y. H.; Pui, D. Y. H. *J. Colloid Interface Sci.* **1974**, *47*, 155. (b) Knutson, E. O.; Whitby, K. T. *J. Aerosol Sci.* **1975**, *6*, 443.

(22) (a) Knutson, E. O.; Whitby, K. T. *J. Aerosol Sci.* **1975**, *6*, 453. (b) Knutson, E. O. In *Fine Particles: Aerosol Generation, Measurement, and Sampling*; Liu, B. Y. H., Ed.; Academic Press: New York, 1976; pp 740−762. (c) Hoppel, W. A. *J. Aerosol Sci.* **1978**, *9*, 41. (d) Kousaka, Y.; Okuyama, K.; Adachi, M. *Aerosol Sci. Technol.* **1985**, *4*, 209.

(23) Fuchs, N. A. *Geofis. Pura Appl.* **1963**, *56*, 185.

(24) (a) Meakin, P.; Donn, B.; Mulholland, G. W. *Langmuir* **1989**, *5*, 510. (b) Schmidt-Ott, A.; Baltensperger, U.; Gäggeler, H. W.; Jost, D. T. *J. Aerosol Sci.* **1990**, *21*, 711. (c) Rogak, S. N.; Baltensperger, U.; Flagan, R. C. *Aerosol Sci. Technol.* **1991**, *14*, 447. (d) Keller, A.; Fierz, M.; Siegmann, K.; Siegmann, H. C.; Filippov, A. *J. Vac. Sci. Technol., A* **2001**, *19*, 1.

(25) Wiedensohler, A. *J. Aerosol Sci.* **1988**, *19*, 387.

(26) Wang, S. C.; Flagan, R. C. *Aerosol Sci. Technol.* **1990**, *13*, 230.

(27) Skillas, G.; Burtscher, H.; Siegmann, K.; Baltensperger, U. *J. Colloid Interface Sci.* **1999**, *217*, 269.